Vanadium(V) Environments in Bismuth Vanadates: A Structural Investigation Using Raman Spectroscopy and Solid State ^{51}V NMR

FRANKLIN D. HARDCASTLE† AND ISRAEL E. WACHS*

Zettlemoyer Center for Surface Studies, Departments of Chemistry and Chemical Engineering, Lehigh University, Bethlehem, Pennsylvania 18015

HELLMUT ECKERT*

Department of Chemistry, University of California, Santa Barbara, Goleta, California 93106

AND DAVID A. JEFFERSON

Department of Physical Chemistry, University of Cambridge, Cambridge, CB2 1EP, United Kingdom

The Bi_2O_3–V_2O_5 system was examined using Raman spectroscopy and solid state ^{51}V wideline, magic-angle spinning (MAS), and nutation NMR spectroscopy. The methods are shown to be complementary in the identification of the various phases and in the characterization of their vanadium site symmetries. Most of the compositions examined ($1:1 \leq Bi:V \leq 60:1$) are multiphasic. Depending on the $Bi:V$ ratio, the following phases have been identified: $BiVO_4$, $Bi_4V_2O_{11}$, a triclinic type-II phase, a cubic type-I phase, γ-Bi_2O_3 doped with V(V) (sillenite), and β-Bi_2O_3. Detailed spectroscopic characterization reveals that vanadium is tetrahedrally coordinated in all these compounds, and that the degree of symmetry increases with increasing $Bi:V$ ratio. At the highest $Bi:V$ ratios, the combined interpretation of the Raman and NMR data provides strong evidence for the presence of $Bi^{5+}O_4$ tetrahedra. © 1991 Academic Press, Inc.

Introduction

The ternary oxides derived from bismuth oxide exhibit a variety of interesting physical properties. For example, the bismuth molybdates are catalytically active in commercially important reactions such as se-

lective oxidations and ammoxidations of alkenes and other hydrocarbons (*1, 2*). The tetragonal phases of thin-film bismuth vanadates and bismuth niobates are efficient photoconductors (*3*). In spite of these remarkable properties, the crystal structures for most of these compounds are not known. This is because of the difficulties encountered with X-ray diffraction in determining the location of oxygen atoms surrounding the metal sites; the X-ray scat-

*To whom correspondence should be addressed.
†Present Address: Sandia National Laboratories, Div. 1845, Albuquerque, NM 87185.

194

tering of the metal cations interferes with the scattering from surrounding oxygen atoms. In view of the potential importance of these systems, a series of studies has been initiated to determine the structures of the ternary bismuth oxides using X-ray powder diffraction, electron diffraction, high-resolution electron microscopy, X-ray absorption near-edge spectroscopy, solid-state NMR spectroscopy, and Raman spectroscopy (4, 5).

Solid-state NMR methods represent a novel and promising approach to determining the local structure of the vanadate species in the bismuth vanadates. Since only the local environment of the nucleus under study is probed by NMR, this method is well suited for the structural analysis of disordered and compositionally complex systems. Solid state wideline, magic-angle spinning (MAS) and pulse excitation (nutation) NMR techniques have recently been used to identify the local environments of two-dimensional vanadium(V) oxide surface layers on titania and alumina supports (6). In addition to the structural information provided by NMR methods, the direct proportionality of the signal intensity to the number of contributing nuclei makes NMR a useful technique for quantitative studies. While ^{27}Al, ^{29}Si, and ^1H MAS NMR have found widespread applications in catalytic systems (7), the scope of previous ^{51}V NMR applications to problems in material science, such as structural studies of catalysts or catalyst-analogue systems, has been limited (6, 8–17). This is especially surprising in view of the highly favorable NMR properties of the ^{51}V isotope ($I = 7/2$), which is 99.76% naturally abundant and has a large magnetic moment and short spin-lattice relaxation times due to the nuclear electric quadrupole interaction.

Raman spectroscopy aids in the elucidation of the structures of transition metal oxides in bulk phases (18, 19) and surface

supported phases (19, 20). The most direct way of determining the structure of an unknown species is by the group frequency approach. The group frequency approach entails comparing the Raman spectrum of the unknown species with that of reference compounds having known structures, and this method works best for molecules having regular structures. For example, characteristic Raman bands have been used to determine the isolated nature of the tetrahedrally coordinated surface rhenium oxide species present on the γ-Al_2O_3 support (21) as well as the mono- and polychromate species present on γ-Al_2O_3, TiO_2, and SiO_2 (22). Recently, however, another approach was developed for determining the structures of vanadium oxide molecules which used an empirical stretching frequency/bond distance correlation (23). The procedure is based on the diatomic approximation in which each V–O bond is considered as an independent oscillator separated from the rest of the molecule or the crystalline lattice. According to the diatomic approximation, the metal oxide polyhedra within the unit cell are reduced to an assembly of metal–oxygen diatomic functionalities. A stretching frequency/bond distance correlation can then be used to determine bond distances in metal oxides from measured Raman stretching frequencies. Thus, Raman spectroscopy can provide fundamental information about the molecular structures and bond lengths of transition metal oxide systems.

In the present study, Raman spectroscopy and field-dependent ^{51}V MAS and wideline MAS and nutation NMR are used to characterize the vanadium(V) environments and determine the structure of the vanadate species in the bismuth vanadates of compositional range $1:1 \leq Bi:V \leq 60:1$. The V–O bond distances of the vanadate species are determined from Raman stretching frequencies using the V–O stretching frequency/bond distance corre-

lation (23). In addition, the bismuth oxide phases are identified by their characteristic Raman bands.

Experimental

The bismuth vanadates were prepared by mixing stoichiometric amounts of α-Bi_2O_3 (99.9%) with V_2O_5 (99.6%). The mixture was ground in acetone with an agate mortar and pestal, dried in air, and then heated at about 825°C for 88–190 hr ($BiVO_4$: 620°C for 195 hr) in a flow of pure oxygen. The samples were then quenched to room temperature. Further details of the preparation are given elsewhere (24).

Raman spectra from the bismuth vanadate samples were generated with the 514.5-nm line of a Spectra-Physics Ar^+ laser (Model 171) utilizing about 10–40 mW of radiant power. The laser intensity was monitored at the sample. The scattered radiation was directed into a Spex Triplemate Spectrometer (Model 1877) which was coupled to an intensified photodiode array (1024 pixels) and optical multichannel analyzer (OMA III: Princeton Applied Research, Model 1463). The photodiode array was thermoelectrically cooled to −35°C. The Raman spectra were collected and recorded using an OMA III dedicated computer and software. The spectral resolution and reproducibility was experimentally determined to be better than 2 cm^{-1}. About 100–200 mg of each sample was pressed into a thin wafer of about 1-mm thickness with a KBr backing. Further details concerning the optical arrangement used in the Raman experiments can be found elsewhere (20).

Wideline and MAS [51]V solid-state nuclear magnetic resonance spectra were obtained at 79.0 and 131.5 MHz, using General Electric GN-300 and GN-500 spectrometers, equipped with multinuclear MAS-NMR probes from Doty Scientific. Pulses of 1-μs length and 1-s relaxation delays were used.

In samples with multiple peaks, the relative peak areas were unchanged when using longer relaxation delays. Typical spinning speeds were 4.0 and 8.0 kHz at the lower and higher field strengths, respectively. Chemical shifts are referenced to $VOCl_3$. For representative samples, nutation NMR studies were carried out at an rf field strength of 27.8 kHz (9 μs liquid 90° pulse), by systematically incrementing the length of the excitation pulse (0.5 to 16 μs in 0.5-μs steps).

Results

Raman Spectroscopy

The Raman spectra for the Bi_2O_3–V_2O_5 samples are presented in Figs. 1–6. Most of the bismuth vanadates studied are multiphasic and this is shown in Table I, which lists the observed Raman frequencies of the various compositions for each of the identified phases. These phases are briefly summarized in this section.

The Raman spectrum of the 1 : 1 composition (Bi_2O_3–V_2O_5) is presented in Fig. 1. A comparison of the powder X-ray diffraction pattern of the 1 : 1 composition with that of pure $BiVO_4$ (25) shows that only $BiVO_4$ is present in the 1 : 1 composition. Thus, the observed Raman bands shown in the spectrum of the 1 : 1 composition, Fig. 1, are assigned to the $BiVO_4$ phase. The Raman bands of $BiVO_4$ are quite distinctive and sharp with the most intense band at 826 cm^{-1}, bands of medium intensity at 366, 320, 210, and 127 cm^{-1}, and a weak band at 700 cm^{-1} (see Table I).

The Raman spectrum of the 2 : 1 composition is shown in Fig. 2. The Raman bands characteristic of the $BiVO_4$ phase are observed at 826, 366, 320, 210, and 127 cm^{-1}. These bands, however, indicate a greater degree of disorder for the average vanadate species because of the observed increase in peak widths and the increase in relative

TABLE I

SUMMARY OF THE Bi_2O_3–V_2O_5 RAMAN RESULTS

Bi:V	Phase	Raman bands (cm^{-1})
1:1	$BiVO_4$	826(vs), 700(w), 366(m), 320(m), 210(m), 127(m)
2:1	$BiVO_4$	826(vs), 716(w), 366(m), 320(m), 210(m), 127(m)
	$(VO_3)_n^{n-}$ (?)	925(w)
	Sillenite:	
	γ-Bi_2O_3	526(m), 266(vw)
	γ-VO_4	790(vw)
4:1	$BiVO_4$	823(vs), 700(vw,br), 363(m), 209(m)
	Type-II	823(vs)
	Sillenite:	
	γ-Bi_2O_3	624(vw), 526(w), ~314(m,br), 266(vw)
	γ-VO_4	790(vw)
	β-Bi_2O_3	314(m,br)
6:1	Type-II	820(vs), 750(m,sh)
	β-Bi_2O_3	314(m), 464(w), 555(w)
	δ-Bi_2O_3 (?)	555(br)
10:1	Type-I	816(vs), 750(w,sh)
	Sillenite:	
	γ-Bi_2O_3	533(w), 271(vw), 213(vw)
	β-Bi_2O_3	303(m)
	δ-Bi_2O_3 (?)	604(br)
19:1	Type-I	821(s,sh)
	Sillenite:	
	γ-Bi_2O_3	619(w), 530(vs), 448(w), 321(s), 267(s), 202(w), 146(m), 128(s)
	γ-VO_4	790(vs), 775(m,sh)
25:1	Sillenite:	
	γ-Bi_2O_3	619(w), 530(vs), 448(w), 321(s), 267(s), 202(w), 146(m), 128(s)
	γ-VO_4	790(vs), 775(m,sh)
	$Bi^{5+}O_4$	827(w)
60:1	Sillenite:	
	γ-Bi_2O_3	619(w), 530(vs), 448(w), 321(s), 267(s), 202(w), 146(m), 128(s)
	γ-VO_4	790(vs), 775(m,sh)
	$Bi^{5+}O_4$	827(m)

Note. Abbreviations used: vs, very strong; s, strong; m, medium; w, weak; vw, very weak; br, broad; sh, shoulder. (?) Denotes questionable existence. The δ-Bi_2O_3 phase might be replaced by an oxygen-deficient β-Bi_2O_3 phase.
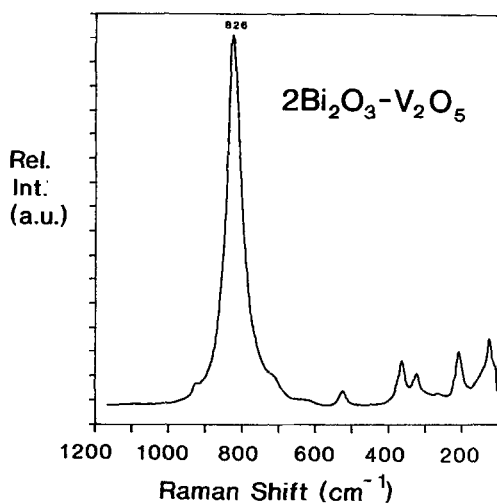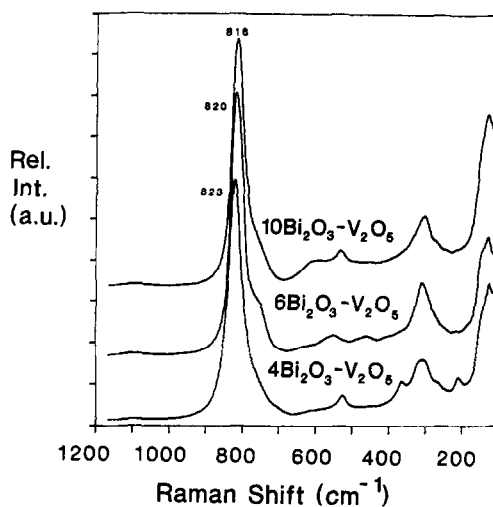
integrated intensities of the band at 826 cm^{-1} compared to those of 366, 320, 210, and 127 cm^{-1}. These observations are also consistent with the superposition of Raman bands due to a second component, $Bi_4V_2O_{11}$ (orthorhombic structure), which was identified by X-ray diffraction (24) to be a major component at the 2:1 composition. The only visual evidence provided by Raman spectroscopy for the presence of $Bi_4V_2O_{11}$

in the 2:1 composition, however, is the asymmetry observed on the low frequency side of the most intense band at 826 cm^{-1} and the shift of the weak band from 700 to 716 cm^{-1}. Both of these observations are consistent with an average increase in the regularity of the VO_4 tetrahedra in the 2:1 composition.

An impurity vanadate species was also identified in the 2:1 composition. The vana-
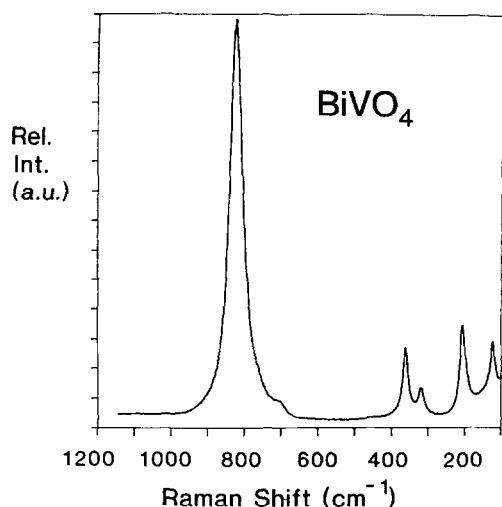
FIG. 1. Raman spectra of BiVO$_4$.

FIG. 3. Raman spectra of 4Bi$_2$O$_3$–V$_2$O$_5$, 6Bi$_2$O$_3$–V$_2$O$_5$, and 10Bi$_2$O$_3$–V$_2$O$_5$ compositions.

date impurity gives rise to a weak band at 925 cm^{-1}. This peak position is the highest observed for the bismuth vanadate samples and reflects a much higher V–O bond order than that found in BiVO$_4$. The impurity cannot be identified, however, because its remaining Raman bands are not observed.

FIG. 2. Raman spectrum of the 2Bi$_2$O$_3$–V$_2$O$_5$ composition.

Furthermore, this species was not identified by other techniques such as NMR and diffraction because of its very low concentration. Given the single data point at 925 cm^{-1}, which reflects the highest V–O bond order, and an assumption that this vanadate species may be very regular, reference to crystalline "model" compounds suggests an assignment to a chain-like structure such as that present in ammonium metavanadate: (VO$_3$)$_n^{n-}$ (26). As Table I shows, the Raman bands due to the sillenite phase are also observed for the 2 : 1 composition; these results will be discussed below.

The Raman spectra for the 4 : 1, 6 : 1, and 10 : 1 compositions are shown in Fig. 3. These compositions have recently been investigated by Zhou using selected-area electron diffraction (SAED) and high-resolution electron microscopy (HREM) (24). These experiments found that the 4 : 1 and 6 : 1 compositions contain a triclinic phase, labelled as the type-II phase, which was found to be the only vanadate phase present in the 6 : 1 composition. The 10 : 1 composition was found to consist of a fluorite-like cubic phase, labelled by Zhou as the type-I phase.

The Raman spectrum of the 6 : 1 composition, which was found by Zhou to contain only the type-II phase (24), shows a very strong Raman band at 820 cm^{-1} and a shoulder of medium intensity at 750 cm^{-1}, both assigned to the VO_4 tetrahedron in the type-II phase. The Raman spectrum of the 4 : 1 composition reflects the presence of $BiVO_4$ and the type-II phase. Characteristic Raman bands for $BiVO_4$ in the 4 : 1 composition are observed at 363 and 209 cm^{-1}, both of medium intensity, along with a very weak band at 700 cm^{-1}. The most intense band in this spectrum occurs at 823 cm^{-1} and reflects the average of the Raman bands due to the two components which are present in the 4 : 1 composition: $BiVO_4$, at 826 cm^{-1}, and the type-II phase, at 820 cm^{-1}. The Raman spectrum of the 10 : 1 composition reflects the presence of the type-I phase (fluorite-like). The most intense band at 816 cm^{-1} of the 10 : 1 composition is assigned to the VO_4 tetrahedron in the type-I phase. Thus, the Raman spectra for the 4 : 1, 6 : 1, and 10 : 1 compositions reflect the various bismuth vanadate phases and the respective VO_4 tetrahedra present in these systems.

The sillenite phase is also present in a few of the bismuth vanadates in the compositional range 2 : 1 ≤ Bi : V ≤ 10 : 1. The sillenite structure is believed to be isomorphous to pure γ-Bi_2O_3, which is metastable and observed at 639°C by cooling from the high-temperature form of δ-Bi_2O_3 (27). At lower temperatures, the γ-Bi_2O_3 phase can be stabilized by a metal cation. The most ideal sillenite structures are those containing quadrivalent metal cations, for example in $Bi_{12}GeO_{20}$ and $Bi_{12}SiO_{20}$ (28), because cations such as Ge^{4+} and Si^{4+} lead to structures containing no vacancies in the sillenite structure. The metal cations occupy perfect tetrahedral sites in the γ-Bi_2O_3 structure. The sillenite structure has also been stabilized by pentavalent metal cations such as P^{5+}, As^{5+}, V^{5+}, and Bi^{5+}, and the Raman spectra of these have been reported (29).
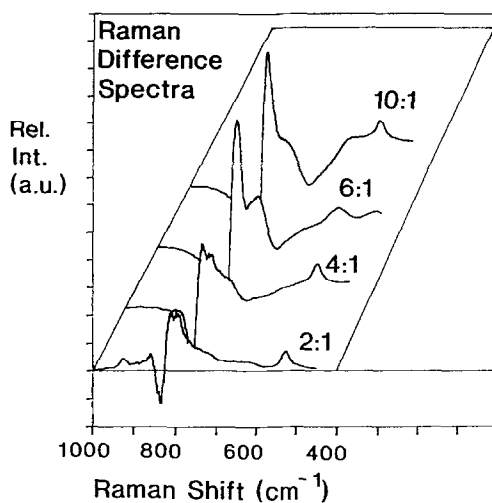

FIG. 4. Raman difference spectra of 2 : 1, 4 : 1, 6 : 1, and 10 : 1 compositions with $BiVO_4$ subtracted from the spectra.

For vanadia-stabilized sillenite, V^{5+} occupies the perfect tetrahedral sites as a VO_4 tetrahedron. For clarity, we refer to this tetrahedron as γ-VO_4 and the corresponding bismuth oxide structure as γ-Bi_2O_3.

The sillenite structure is identified in the 2 : 1, 4 : 1, and 10 : 1 compositions by comparing the Raman spectra in Figs. 2 and 3 with those of vanadia-stabilized sillenite compounds (29, 30). The Raman band of medium intensity at 526 cm^{-1} and the weak band at 266 cm^{-1} is diagnostic of the γ-Bi_2O_3 structure in sillenite. The bands due to γ-Bi_2O_3 are more prominent for the 4 : 1 composition at 528, 314, and 267 cm^{-1}, and a very weak band at 624 cm^{-1}. The 10 : 1 composition exhibits weaker bands at 533, 271, and 213 cm^{-1} due to γ-Bi_2O_3. Thus, the sillenite phase is detected in the 2 : 1, 4 : 1, and 10 : 1 compositions by characteristic Raman bands due to the γ-Bi_2O_3 structure within the sillenite.

The Raman difference spectra of the 2 : 1, 4 : 1, 6 : 1, and 10 : 1 compositions, shown in Fig. 4, yield further information about the phases present in these samples. The differ-

ence spectra result from subtraction of the
spectrum of BiVO$_4$ from the spectra of the
2:1, 4:1, 6:1, and 10:1 compositions. The
purpose of the subtraction is to accentuate
the weaker non-BiVO$_4$ spectral details
which remain hidden in the spectra of Figs.
2 and 3. The difference spectra for the 2:1
and 4:1 compositions reveal the presence
of a weak band at 790 cm^{-1}. This weak band
at 790 cm^{-1} is identified as the γ-VO$_4$ tetra-
hedron, which occupies the perfect tetrahe-
dral sites within the sillenite structure. The
790-cm^{-1} band is not observed in the Raman
spectra of the 6:1 and 10:1 compositions.
This is expected for the 6:1 composition
where the Raman bands of γ-Bi$_2$O$_3$ were
not observed and diffraction shows only the
type-II phase. For the 10:1 composition,
however, where the Raman bands of γ-
Bi$_2$O$_3$ were observed, the 790-cm^{-1} band is
overwhelmed by the bands due to the type-
I phase. Thus, the Raman difference spectra
substantiate the presence of the sillenite
phase in the 2:1 and 4:1 compositions by
revealing the V–O stretch at 790 cm^{-1} due
to the γ-VO$_4$ tetrahedron.

The Raman spectra in Fig. 3 show that the
major bismuth oxide phase present in the
4:1, 6:1, and 10:1 compositions is β-Bi$_2$O$_3$
(tetragonal). β-Bi$_2$O$_3$ has been reported to
be metastable, but may be observed in its
pure form at 650°C on cooling from δ-Bi$_2$O$_3$
(high-temperature phase), or stabilized to
room temperature by the addition of small
amounts of a cation impurity (27). The β-
phase of Bi$_2$O$_3$ has been identified by Raman
spectroscopy in Ta- and Nb-stabilized struc-
tures to have two major bands at 311 and
462 cm^{-1} (30).

The Raman spectra of the 4:1, 6:1, and
10:1 compositions, Fig. 3, show the pres-
ence of β-Bi$_2$O$_3$ in all of these compositions
with the possible presence of δ-Bi$_2$O$_3$ in the
6:1 and 10:1 compositions. The Raman
spectrum of the 4:1 composition shows a
broad band at 314 cm^{-1}, which hints at the
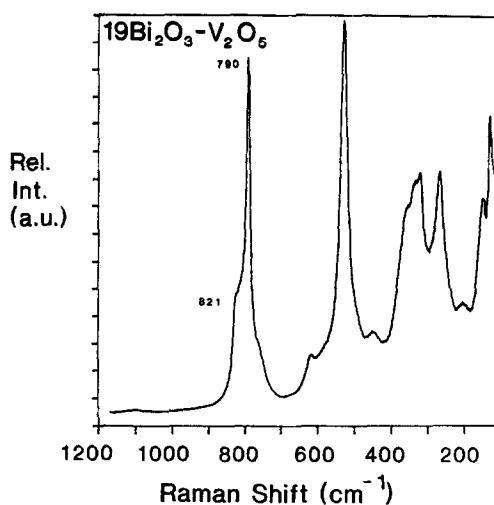presence of β-Bi$_2$O$_3$, although this band

FIG. 5. Raman spectrum of the 19Bi$_2$O$_3$–V$_2$O$_5$ compo-
sition.

overlaps severely with bands due to the co-
existing sillenite and BiVO$_4$ phases. The β-
Bi$_2$O$_3$ phase is also identified at the 6:1 com-
position by Raman bands at 314 and 464
cm^{-1}. The broad band at 555 cm^{-1}, how-
ever, may be attributed to the presence of
the δ-phase of Bi$_2$O$_3$ (30) instead of β-Bi$_2$O$_3$.
Alternatively, this band may arise from an
oxygen-deficient bismuth oxide structure,
for example β-Bi$_2$O$_{2.5}$ (31), where the BiO$_6$
structural units of the β-Bi$_2$O$_3$ lattice are
converted to BiO$_4$ units because of oxygen
vacancies; the BiO$_4$ unit is expected to ex-
hibit a stretching frequency at ~570 cm^{-1}
(30). At the 10:1 composition, the band at
303 cm^{-1} is assigned to β-Bi$_2$O$_3$, and the
broad band at 604 cm^{-1} may indicate the
presence of δ-Bi$_2$O$_3$ or an oxygen-deficient
β-Bi$_2$O$_3$. Thus, the β-Bi$_2$O$_3$ phase, a tetrago-
nal structure of bismuth oxide, is identified
by characteristic Raman bands in the 4:1,
6:1, and 10:1 compositions. In addition,
the possible presence of δ-Bi$_2$O$_3$, or an oxy-
gen-deficient β-Bi$_2$O$_3$ phase, is noted in the
6:1 and 10:1 compositions.

The Raman spectra of samples with high
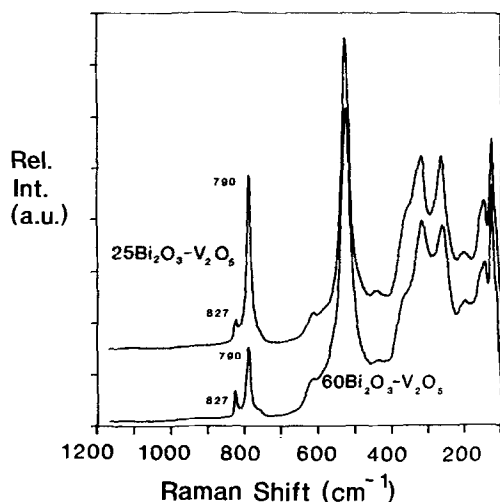Bi:V compositions are shown in Figs. 5 and

FIG. 6. Raman spectra of $25Bi_2O_3$–V_2O_5 and $60Bi_2O_3$–V_2O_5 compositions.

6. The Raman spectrum of the 19 : 1 sample, Fig. 5, shows bands due to two distinct types of VO_4 tetrahedra as well as γ-Bi_2O_3. The most pronounced V–O stretching mode is at 790 cm^{-1}, with an accompanying stretching mode at 775 cm^{-1}, both due to γ-VO_4 in the sillenite structure. The γ-Bi_2O_3 phase has well-defined Raman bands at 619(w), 530(vs), 448(w), 321(s), 267(s), 202(w), 146(s), and 128(s) cm^{-1}. The second VO_4 tetrahedron in the 19 : 1 composition gives rise to the shoulder at 821 cm^{-1}. The assignment of the 821-cm^{-1} band is unclear because of its strong overlap with the intense band at 790 cm^{-1} and cannot be made from the Raman data alone. The ^{51}V NMR data, to be presented in the next section, shows a very broad feature in the spectrum of the 19 : 1 composition consistent with that observed for the dominant phase in the 10 : 1 composition. Hence, the shoulder appearing at 821 cm^{-1} in the Raman spectrum of the 10 : 1 composition, Fig. 5, is assigned to the type-I phase (V–O stretch at 816 cm^{-1}), which dominates in the 10 : 1 composition.

The Raman spectra of the 25 : 1 and 60 : 1 compositions are presented in Fig. 6 and

appear quite similar to the Raman spectrum of the 19 : 1 composition, except that the type-I phase is no longer present. Both the 25 : 1 and the 60 : 1 compositions exhibit Raman bands characteristic of γ-Bi_2O_3 and the accompanying γ-VO_4 tetrahedron. In addition, however, a sharp Raman band is present in each of these spectra at 827 cm^{-1}. As the Bi : V composition is changed from 25 : 1 to 60 : 1, the 790-cm^{-1} band decreases in relative intensity while the 827-cm^{-1} band increases in relative intensity. In conjunction with the NMR data, to be discussed below, we propose that the Raman band at 827 cm^{-1} is due to the Bi–O stretch from a $Bi^{5+}O_4$ tetrahedron.

^{51}V NMR

Extensive model compound studies have previously shown that the ^{51}V chemical shift anisotropy (which can be obtained from wideline NMR) is the most reliable spectroscopic parameter for differentiating between the various basic V(V) coordination types (6). For the compounds of the present investigation, the wideline NMR spectra show that the chemical shift anisotropies in all of the samples are either near zero or fairly small (less than 200 ppm). These results indicate that all of the vanadium sites in the present materials are four-coordinate. The small chemical shift anisotropies are most consistent with isolated VO_4 tetrahedra ($Q^{(0)}$ species), although the presence of $Q^{(1)}$ species (containing one V–O–V bond) cannot be ruled out with certainty.

Further site discrimination is provided by the MAS-NMR spectra, shown in Fig. 7, in which chemically distinct VO_4 tetrahedra are differentiated by unique chemical shift values. The peaks marked by asterisks in the spectra arise from the $2I$-1 outer NMR transitions which are broadened by the anisotropy of first-order quadrupolar perturbations and are converted into a spinning sideband pattern upon MAS. In the case of very strong quadrupolar interactions the outer
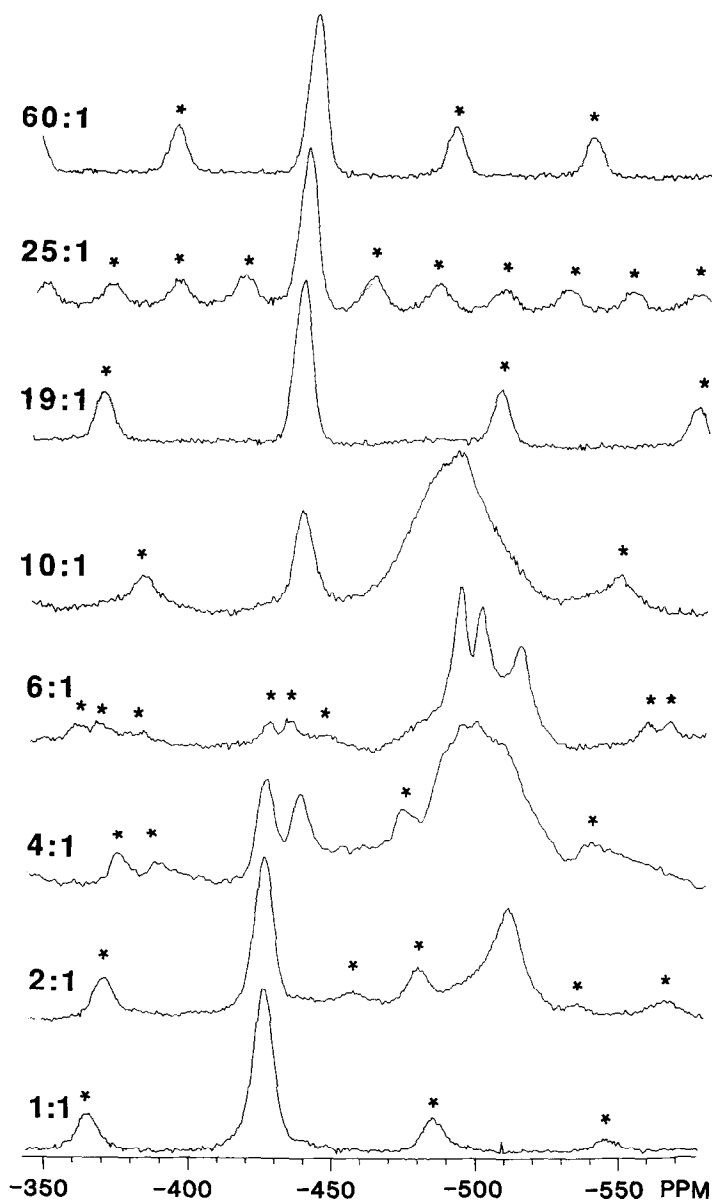
FIG. 7. 131.5-MHz ^{51}V MAS–NMR spectra of Bi_2O_3–V_2O_5 phases. The atomic Bi:V ratios are indicated. Spinning sidebands are shown by asterisks.

transitions can be broadened over such a wide spectral region that their excitation by the radiofrequency pulse becomes incomplete. It has been shown that, as a consequence, the length of the effective 90° pulse is reduced (32). For ^{51}V ($I = 7/2$), under the chosen experimental conditions, its value can range from 9 μs (nonselective excitation, zero quadrupolar interaction) to 2.25 μs (entirely selective excitation, strong

quadrupolar interaction). For ^{51}V in the solid state intermediate values are common, indicating that the outer transitions are at least partially excited. The degree of excitation is selectively probed in the so-called nutation NMR experiment where the signal intensity is measured as a function of pulse length. Figure 8 shows some representative data, resulting in the effective 90° pulse lengths listed in Table II.

The nuclear electric quadrupole interaction has been characterized further by field-dependent MAS-NMR. Large quadrupolar interactions will manifest themselves in upfield resonance displacements ("second-order quadrupole shifts") that increase with decreasing external field strength. For all samples with Bi : V ratios exceeding 4 : 1, however, the ^{51}V resonance shifts at 7.0 and 11.7 T (see Table II) are found to be identical within experimental error. From this result we can estimate an upper limit of ca. 1 MHz for the nuclear electric quadrupole coupling constant, a rather small value indicative of quite symmetric vanadium(V) environments. In contrast, the larger field dependencies of the ^{51}V resonances in BiVO$_4$ and Bi$_4$V$_2$O$_{11}$ indicate much higher asymmetries.

The ^{51}V MAS-NMR spectra of the bismuth vanadate samples, presented in Fig. 7, are briefly described. The spectrum of the 2 : 1 composition shows the presence of two quite symmetric vanadium sites which are four-coordinate and have $Q^{(0)}$ environments. These peaks occur at −425.6 and −510.0 ppm and are approximately equivalent in their integrated peak areas showing that these two species are present in about a 1 : 1 concentration ratio. The sharp peak at −425.6 ppm is identified as BiVO$_4$, while the peak at −510.0 ppm is much broader and represents the VO$_4$ tetrahedron in Bi$_4$V$_2$O$_{11}$.

The ^{51}V MAS-NMR spectrum of the 4 : 1 composition shows at least three symmetric vanadium sites which are four-coordinate and have $Q^{(0)}$ environments. The two sharp peaks at −425.8 and −437.8 ppm are identi-

fied as small quantities of BiVO$_4$ and sillenite, respectively. The very large and broad peak at −493 ppm appears to be a complex mixture of VO$_4$ tetrahedra present in the type-II phase. The type-II phase is the only bismuth vanadate present in the 6 : 1 composition (24).

The ^{51}V MAS-NMR spectrum of the 6 : 1 composition shows a well-defined set of three peaks at −492.7, −499.8, and −513.4 ppm which are due to the type-II phase. These three peaks indicate the presence of three crystallographically distinct tetrahedral vanadium sites (area ratio approximately 1 : 1 : 1), which are fairly symmetric. The phase purity of this sample is confirmed by the absence of peaks due to the BiVO$_4$ and sillenite phases.

The ^{51}V MAS-NMR spectrum of the 10 : 1 composition shows a sharp peak at −438.0 ppm, due to γ-VO$_4$ of the sillenite phase, and a rather strong, broad peak at −492 ppm. The broad peak at −492 ppm represents the chemical shift of the isolated VO$_4$ tetrahedron present in the type-I phase.

The ^{51}V MAS-NMR spectra of the higher Bi : V compositions show the presence of sillenite as the dominant phase. The spectrum of the 19 : 1 composition shows only a sharp peak at −437.8 ppm, which is due to the sillenite phase. Wideline NMR studies, however, show an additional broader component around −490 ppm corresponding to the peak observed for the type-I phase in the 10 : 1 composition. This peak is not clearly resolved in Fig. 7 because of the intrinsically large width and the dominance of the γ-VO$_4$ resonance. The ^{51}V MAS-NMR spectrum of the 25 : 1 and 60 : 1 compositions shows only a sharp peak due to the phase purity of the sillenite phase at these compositions.

The combined Raman and NMR results are shown in Table III and demonstrate the complementary nature of the two techniques in discerning bismuth vanadate and bismuth oxide phases in the Bi$_2$O$_3$–V$_2$O$_5$ system. In this table, the R and N designa-
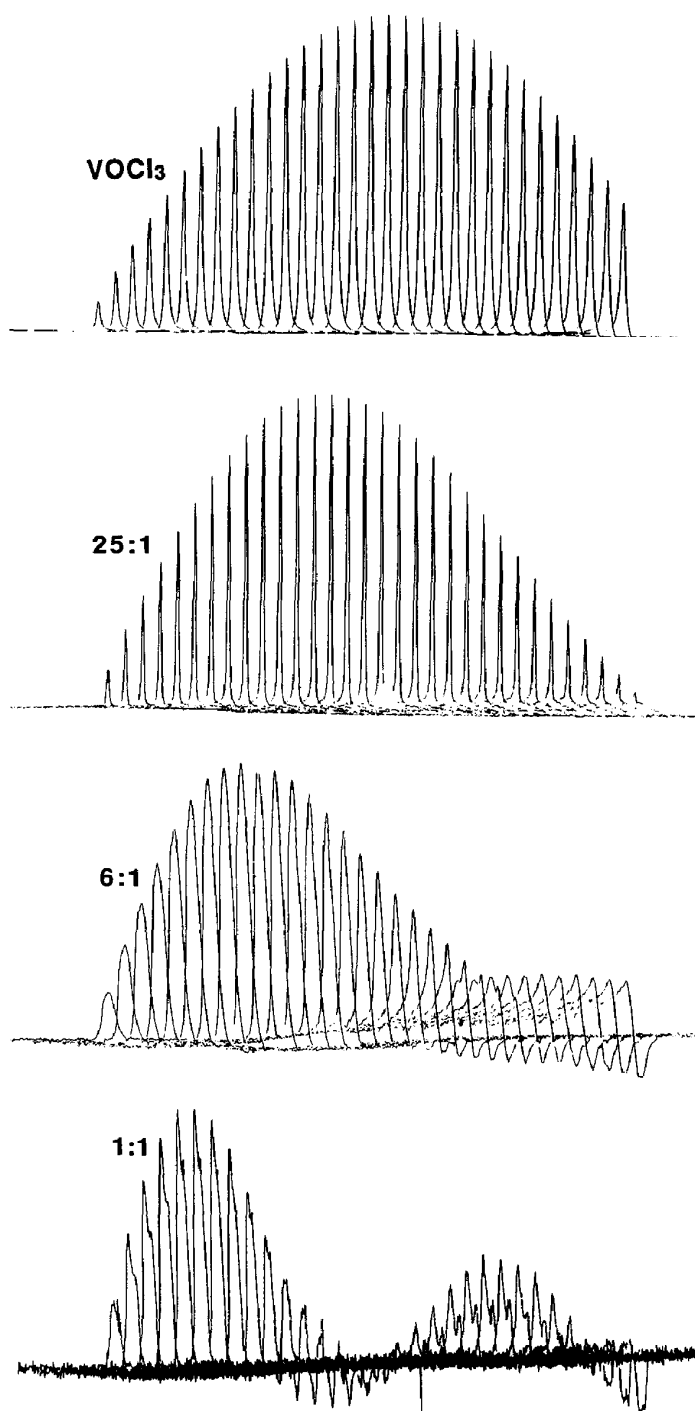
VOCl₃

25:1

6:1

1:1

FIG. 8. Representative ^{51}V Nutation NMR on nonspinning samples at a rf field strength of 27.8 kHz. Shown are collections of Fourier transforms as a function of pulse length in 0.5 μs increments, starting with 0.5 μs and ending with 16 μs.

Sample	δ^a (7.05 T) (ppm)	δ(11.7 T) (ppm)	$t_p(90°)^b$ (μs)
60 : 1	−441.4	−441.5	
25 : 1	−439.3	−439.1	7.0
19 : 1	−438.1	−437.8	
10 : 1	−437.6	−438.0	
	−486 ± 2	−492 ± 2	5.5
6 : 1	−493.1	−492.7	4.8
	−500.7	−499.8	4.8
	−512.9	−513.4	4.8
4 : 1	−437.5	−425.8 (BiVO₄)	
		−437.8	
	−492 ± 2	−493 ± 2	
2 : 1	−434 ± 1^c	−425.6 (BiVO₄)	
	−512.6	−510.0	
1 : 1	−432.8	−425.6 (BiVO₄)	2.8

^{a} In ppm vs VOCl₃; ±0.5 ppm unless indicated otherwise.

^{b} $t_p(90°)$ refers to the pulse length required for maximum signal observation.

^{c} Poorly resolved.

tions refer to phases identified by Raman and NMR spectroscopies, respectively. The lattice structure for each of these compositions, as determined by Zhou (24), is also included.

Discussion

While the previous section was devoted mainly to the phase compositions and the corresponding spectral assignments for the samples under investigation, in this section the details of the vanadium coordination that can be inferred from the combined interpretation of the Raman and NMR data will be discussed.

The Raman spectra of the bismuth vanadates are interpreted according to the diatomic approximation (23). The diatomic approximation assumes that all the V–O bonds sharing a common vanadium cation are vibrationally independent of one another. Consequently, to a first approxima-

tion, the Raman spectrum is a superposition of V–O stretching frequencies. The V–O stretching frequency is a function of only the V–O bond length. Thus, the V–O bond distance can be determined directly from a measured V–O stretching frequency. The following empirical relationship has been established (23) and expresses V–O bond length R as a function of measured Raman stretching frequency ν(cm^{-1}):

$$R = 0.52148 \ln(21{,}349/\nu(\text{cm}^{-1})). \tag{1}$$

Equation (1) yields a precision of ±0.019 Å for a V–O bond distance R from an observed Raman stretching frequency ν(cm^{-1}).

BiVO₄

BiVO₄ crystallizes in the monoclinic space group $I2/b$, with lattice constants $a = 5.1956(1)$, $b = 5.0935(1)$, $c = 11.7045$ Å, $\gamma = 90.383(1)°$ (25). There is one type of BiO₈ polyhedron and one type of VO₄ tetrahedron, with two sets of V–O bonds of 1.69(2) and 1.77(2) Å. The Raman spectrum of BiVO₄, Fig. 1, reflects the structure of the VO₄ tetrahedron. Although the factor group symmetry of the unit cell is C_{2h}, the site symmetry of each V cation is at most C_2. If C_2 site symmetry is assumed for the V cation (33), then the most intense Raman band at 826 cm^{-1} is assigned to the symmetric V–O stretching mode (A_g symmetry), the weak band at 716 cm^{-1} is assigned to the antisymmetric V–O stretch (B_g symmetry), the symmetric (A_g) and antisymmetric (B_g) bending modes are at 366 and 320 cm^{-1}, respectively, and external modes (rotation/translation) occur at 210 and 127 cm^{-1}. Alternatively, if the diatomic approximation is used (no site symmetry), and Eq. (1) is used to correlate V–O bond distances with stretching frequencies, then both Raman bands at 826 and 716 cm^{-1} are due to stretches of distinct V–O bonds of 1.70(2) and 1.77(2) Å, respectively. These bond distances, deter-

TABLE III

BISMUTH VANADATE AND BISMUTH OXIDE/PHASES PRESENT IN THE COMPOSITIONAL RANGE $1:1 \leq$ Bi:V $\leq$ 60:1 (NOTE: BOXES REFER TO DOMINANT PHASES)

| | Bismuth vanadate phases[a] | | | | | Bi_2O_3 phases | | | |
Bi:V	$BiVO_4$	$Bi_4V_2O_{11}$	Type II	Type I	Sillenite	β	$\delta(?)$	γ	Lattice structure
1:1	R,N								Monoclinic
2:1	R,N	N			R^b			R^b	Orthorhombic
4:1	R,N		R,N		R,N	R		R	Triclinic
6:1			R,N^c			R	R		Triclinic
10:1				R,N	N	R	R	R	fcc
19:1				(R),N^d	R,N			R	bcc + fcc
25:1					R,N			R	bcc
60:1					R,N			R	bcc

[a] R, identified by Raman spectroscopy; N, identified by ^{51}V MAS-NMR.

[b] Trace levels.

[c] Three crystallographically distinct VO_4 tetrahedra were identified by ^{51}V MAS-NMR.

[d] Detected by wideline ^{51}V NMR as a broad shoulder; the Raman band for the type-I phase is detected, but cannot be identified by Raman alone because of strong overlap with the band at 790 cm^{-1} due to γ-VO_4.

mined from the Raman spectrum, are very close to the crystallographically determined bond distances of 1.69(2) and 1.77(2) Å (25).

Of the various VO_4 tetrahedra identified within the Bi_2O_3-V_2O_5 system, that present in $BiVO_4$ is the least symmetric. The asymmetry is reflected in the Raman spectra, where the V–O symmetric stretch occurs at the highest wavenumber, in the field-dependence of the MAS-NMR resonance shift, as well as the high degree of excitation selectivity.

$Bi_4V_2O_{11}$

Recent investigations into the structure of $Bi_4V_2O_{11}$ have led to contradictory results (34–36). Abraham (34) used single crystal X-ray diffraction to measure the lattice parameters of the orthorhombic cell as $a = 16.599(4)$, $b = 5.611(1)$, and $c = 15.288(4)$ Å. The existence of $Bi_2O_2^{2+}$ layers was confirmed and the location of the vanadium atoms was determined to be similar to that of the Mo atom in γ-Bi_2MoO_6. The compound $Bi_4V_2O_{11}$ was consequently formulated as $(Bi_2O_2)^{2+}(VO_{3.5}\square_{0.5})^{2-}$, although it was not

possible with the data collected from twinned crystals to establish the actual structure. On the other hand, Zhou (24) found SAED patterns and HREM images to be very different from those of γ-Bi_2MoO_6, confirming that $Bi_2O_2^{2+}$ layers do not exist in $Bi_4V_2O_{11}$. Instead, the structure is similar to that of the high-temperature modification of bismuth molybdate, γ'-Bi_2MoO_6 (which possesses MoO_4 tetrahedra), which shows a structural relationship closer to fluorite than to perovskite (35, 36).

On the basis of the Raman and NMR spectroscopic evidence, the vanadium environment in $Bi_4V_2O_{11}$ is 4-coordinate. Regarding the symmetry of coordination, Raman and NMR spectra are not entirely in accord with each other. While the position of the Raman band is indistinguishable from that of $BiVO_4$, suggesting a similar site symmetry, the less-pronounced field dependence of the NMR spectra indicates significantly weaker quadrupolar interactions in $Bi_4V_2O_{11}$. We therefore conclude that the NMR spectra appear in this case to be more sensitive to subtle changes in the vanadium coordina-

tion geometry. Furthermore, $BiVO_4$ and $Bi_4V_2O_{11}$ are substantially chemically shifted from each other in the ^{51}V MAS-NMR spectra. The information content of this shift is unclear, however, since at the present time ^{51}V chemical shift values are poorly understood.

Type-II and Type-I Phases

The Raman spectra of Fig. 3 for the samples with Bi : V = 4 : 1, 6 : 1, and 10 : 1 show a continuous shift of the highest frequency band from 823 to 816 cm^{-1}. This continuos shift to lower wavenumber reveals that the average VO_4 tetrahedra becomes more regular as the Bi : V ratio is increased. The symmetric stretch of a perfect VO_4 tetrahedron is expected to occur at 796 ($\pm$20) cm^{-1} (23).

For the type-II phase, Zhou (24) has suggested the presence of a V_4O_{10} pyrochlore unit consisting of four corner-sharing VO_4 tetrahedra with each tetrahedron having three bridging V–O–V groups and one terminal V=O bond. Such mono–oxo vanadate species, however, would exhibit V=O stretching bands near or greater than 1000 cm^{-1} [for example, V_2O_5: 994 cm^{-1}; $V_{10}O_{28}^{6-}$(aq): 1000 cm^{-1}; $VO(OCH_2 CH_2CH_3)_3$: 1073 cm^{-1} (23)]. The observed V–O stretching modes for all vanadate species examined (except for the very small impurity band at 925 cm^{-1} in the 2 : 1 composition) lie at or below 826 cm^{-1}, which clearly excludes the possibility of the V_4O_{10} pyrochlore unit suggested by Zhou. The presence of the pyrochlore V_4O_{10} unit is therefore not substantiated from the Raman data in any of the bismuth vanadates examined.

Both the Raman and the NMR spectroscopic parameters for the type-II phase (predominant constituent in the 4 : 1 and 6 : 1 samples) and the type-I phase (predominant constituent in the 10 : 1 sample) are found to be quite similar, hence underscoring the close structural relationship between both phases. The solid state MAS-NMR spec-

trum of the phase-pure type-II material (6 : 1 sample) shows the presence of three crystallographically distinct tetrahedral vanadium sites, whereas the broad MAS-NMR peaks observed in the 4 : 1 sample and the type-I phase in the 10 : 1 sample indicate that the phases are structurally ill-defined here. This conclusion is in excellent agreement with the Raman spectra, which show that the bands due to the V–O stretching modes in the 4 : 1 and 10 : 1 samples are broadened (Fig. 3), indicating a greater distribution of VO_4 structures.

Sillenite Phase

According to Zhou's X-ray study (24), compositions with higher Bi : V ratios are phase pure, containing only γ-Bi_2O_3 (sillenite). The unit cell of this compound was found to be body-centered cubic with lattice parameter a = 10.2 Å. The structure can accommodate variable amounts of VO_4 tetrahedra, up to a limiting composition of $Bi_{25}VO_{40}$ (Bi : V = 25 : 1). When the vanadium content is less, as for example in $Bi_{25+x}V_{1-x}O_{40}$, xBi^{5+} cations are expected to occupy the remainder of the tetrahedral sites (24, 34, 37).

Both the Raman and the NMR studies reveal that the VO_4 tetrahedra present in γ-Bi_2O_3 are nearly perfect. The Raman band position at 790 cm^{-1} is consistent with that predicted for an ideal tetrahedron (796 cm^{-1}) (23), and the NMR nutation behavior shows essentially nonselective excitation. Thus, both experiments independently show that the degree of symmetry for the VO_4 tetrahedon in the sillenite phase is higher than for any other vanadate compound studied to date by either technique. The NMR spectra show a continuous change of the chemical shift with increasing vanadium concentration, from −441 to −438 ppm, indicating that the chemical bonding state is affected by the degree of vanadium substitution. This compositional evolution further confirms that the vana-

TABLE IV

V–O Bond Distances for VO_4 Tetrahedra in Bismuth Vanadate Phases

Phase	V–O (± 0.019 Å)	No. of V Sites
$BiVO_4$	(3×) 1.696	1
	(1×) 1.782	
$Bi_4V_2O_{11}$	(3×) 1.696	1
	(1×) 1.782	
Type-II	(3×) 1.698	3
	(1×) 1.746	
Type-I	(3×) 1.702	1
	(1×) 1.746	
Sillenite	(4×) 1.719	1

Note. All bond distances calculated from the diatomic approximation: Eq. (1). Number of distinct VO_4 tetrahedra are determined by ^{51}V NMR-MAS

dium content in the sillenite phase can cover a wide range of stoichiometries, rather than constituting the single compound $Bi_{25}VO_{40}$. In combination with the NMR data, which show that only a single vanadate species is present, the second Raman band at 827 cm^{-1} must be due to a Bi–O stretching frequency. Since the wavenumber is too high for a Bi^{3+} oxide species, the combined Raman and NMR data constitute strong evidence for the formation of tetrahedrally coordinated Bi^{5+} sites in the lattice. From an empirically derived Bi–O bond distance/stretching frequency relationship (30), the Bi–O distance is estimated to be about 1.9 Å. Furthermore, the $Bi^{5+}O_4$ tetrahedron is expected to be nearly perfect, consistent with that of the $V^{5+}O_4$ tetrahedron it replaces.

V–O Bond Distances

The V–O bond distances for the VO_4 tetrahedra present in the five identified phases are listed in Table IV. The bond distances are determined from the Raman stretching frequencies and Eq. (1). In addition, the calculated valence state is used as a bookkeep-

ing device for the number of valence electrons and aids in the assignment of the number of V–O bonds of a given bond length (and given valency) (38). The calculated valence state of the V^{5+} cation is 5.0 ± 0.1 v.u. (23).

The V–O bond distances were determined by first converting all V–O stretching frequencies to bond orders. For $BiVO_4$ and $Bi_4V_2O_{11}$ these are 1.320 and 1.026 v.u., for the type-II phase 1.3125 and 1.386 v.u., for the type I phase 1.2969 and 1.1386 v.u., and for sillenite 1.2328 and 1.1968 v.u. These V–O bond orders constitute each respective VO_4 tetrahedron. In order to determine the number of different types of bonds per VO_4 tetrahedron, these bond orders were summed, and those groups of bond orders which add to 5.0 ± 0.1 v.u. were selected as the most probable structure for each phase. For example, for $BiVO_4$ the most probable structure is composed of three bonds of order 1.3204 v.u. and one bond of order 1.026 v.u. which sum to a calculated valence state of 5.0 v.u. This procedure was repeated for all the bismuth vanadate phases. The Raman stretching frequencies were then expressed as bond distances by Eq. (1).

Conclusions

The Bi_2O_3–V_2O_5 system has been examined using Raman spectroscopy and solid state ^{51}V wideline, MAS, and nutation NMR spectroscopy. Five distinct vanadium-containing phases have been identified and the compositional regions of their existence established. The Raman and NMR spectroscopic observables permit further characterization of the vanadium(V) environments in these phases. Both methods independently show that the VO_4 tetrahedra become increasingly symmetric as the Bi : V ratio of the phases increases. Thus, the order of increasing symmetry is $BiVO_4$ < $Bi_4V_2O_{11}$ < type-II phase < type-I phase < γ-VO_4 in γ-Bi_2O_3 (sillenite). The type-I and type-II

phases appear prone to structural disorder and may also be variable in vanadia content. The γ-VO_4 tetrahedra in the sillenite structure are the most symmetric ones known to date. The combined NMR and Raman investigation illustrates further that at vanadia contents lower than those corresponding to the $Bi_{25}VO_{40}$ stoichiometry, the empty sites in the lattice are occupied by highly symmetric $Bi^{5+}O_4$ units.

The results of the present study illustrate the power of this combined Raman/NMR approach toward elucidating the phase composition and site symmetries in complex systems. The power of the NMR method lies in its element selectivity and the inherently quantitative response. Furthermore, NMR parameters appear more sensitive toward subtle changes in coordination geometries than Raman spectroscopy. On the other hand, the information about site symmetries available from NMR is rather qualitative, because currently no reliable theoretical methods or empirical correlations are known that would permit a quantitative interpretation of NMR chemical shifts or nuclear electric quadrupole coupling constants. Here, the diatomic approximation employed in the interpretation of the Raman data has proven extremely useful in deriving V–O bond lengths from Raman stretching frequencies in the compounds under study. The approach of the present investigation has also proven highly informative in the structural analysis of surface vanadia phases on oxide supports currently under investigation in our laboratories (6, 39).

Acknowledgments

References

1. J. M. THOMAS, D. A. JEFFERSON, AND G. R. MILL-WARD, *JEOL News* **23E**, 7 (1985).
2. D. A. JEFFERSON, J. M. THOMAS, M. K. UPPAL, AND R. K. GRASSELLI, *J. Chem. Soc. Chem. Commun.*, 594 (1983).
3. T. SEKIYA, A. TSUZUKI, AND Y. TORII, *Mater. Res. Bull.* **20**, 1383 (1985).
4. F. D. HARDCASTLE, I. E. WACHS, D. J. BUTTREY, D. A. JEFFERSON, AND J. M. THOMAS, in preparation.
5. Z. WUZONG, D. A. JEFFERSON, M. ALARIO-FRANCO, AND J. M. THOMAS, *J. Phys. Chem.* **91**, 512 (1987).
6. H. ECKERT AND I. E. WACHS, *J. Phys. Chem.* **93**, 6796 (1989).
7. T. M. DUNCAN AND C. R. DYBOWSKI, *Surf. Sci. Rep.* **1**, 157 (1981).
8. V. M. MASTIKHIN, O. B. LAPINA, V. N. KRASILNI-KOV, AND A. A. IVAKIN, *React. Kinet. Catal. Lett.* **24**, 119 (1984).
9. V. M. MASTIKHIN, O. B. LAPINA, AND L. G. SIMONOVA, *React. Kinet. Catal. Lett.* **24**, 127 (1984).
10. T. P. GORSHKOVA, R. I. MAKSIMOVSKAYA, D. V. TARASOVA, N. N. CHUMACHENKO, AND T. A. NIKORO, *React. Kinet. Catal. Lett.* **24**, 107 (1984).
11. H. ECKERT AND I. E. WACHS, *Mater. Res. Soc. Symp. Proc.* **111**, 455 (1988).
12. L. R. LE COSTUMER, B. TAOUK, M. LE MEUR, E. PAYEN, M. GUELTON, AND J. GRIMBLOT, *J. Phys. Chem.* **92**, 1230 (1988).
13. B. TAOUK, M. GUELTON, J. GRIMBLOT, AND J. P. BONNELLE, *J. Phys. Chem.* **92**, 6700 (1988).
14. O. B. LAPINA, A. V. SIMAKOV, V. M. MASTIKHIN, S. A. VENIAMINOV, AND A. A. SHUBIN, *J. Mol. Catal.* **50**, 55 (1989).
15. K. V. R. CHARY, V. V. RAO, AND V. M. MASTIK-HIN, *J. Chem. Soc. Chem. Commun.*, 202 (1989).
16. H. ECKERT, G. DEO, I. E. WACHS, AND A. M. HIRT, *Colloids Surf.* in press.
17. C. SANCHEZ, M. NABAVI, AND F. TAULELLE, *Mater. Res. Soc. Symp. Proc.* **121**, 93 (1988).
18. K. NAKAMOTO, "Infrared and Raman Spectra of Inorganic and Coordination Compounds, 3rd ed., Wiley, New York (1978).
19. L. DIXIT, D. L. GERRARD, AND H. J. BOWLEY, *Appl. Spectrosc. Rev.* **22**, 189 (1986).
20. I. E. WACHS, F. D. HARDCASTLE, AND S. S. CHAN, *Spectrosc.* **1(8)**, 30 (1986).
21. F. D. HARDCASTLE, I. E. WACHS, J. A. HORSLEY, AND G. H. VIA, *J. Mol. Catal.* **46**, 15 (1988).
22. F. D. HARDCASTLE AND I. E. WACHS, *J. Mol. Catal.* **46**, 173 (1988).
23. F. D. HARDCASTLE AND I. E. WACHS, *J. Phys. Chem.* in press.
24. W. ZHOU, *J. Solid State Chem.* **76**, 290 (1988).
25. A. W. SLEIGHT, H.-Y. CHEN, A. FERRETTI, AND D. E. COX, *Mater. Res. Bull.* **14**, 1571 (1979).

26. H. T. EVANS, JR., *Z. Kristallogr.* **114,** 257 (1960).

27. H. A. HARWIG, *Z. Anorg. Allg. Chem.* **444,** 151 (1978).

28. S. C. ABRAHAMS, P. B. JAMIESON, AND J. L. BERNSTEIN, *J. Chem. Phys.* **47,** 4034 (1967).

29. M. DEVALETTE, J. DARRIET, M. COUZI, C. MAZEAU, AND P. HAGENMULLER, *J. Solid State Chem.* **43,** 45 (1982).

30. F. D. HARDCASTLE AND I. E. WACHS, to be submitted.

31. A. A. ZAV'YALOVA AND R. M. IMAMOV, *Sov. Phys. Crystallogr.* **16,** 437 (1971).

32. D. FREUDE, J. HAASE, J. KLINOWSKI, T. A. CARPENTER, AND G. RONIKIER, *Chem. Phys. Lett.* **119,** 365 (1985).

33. W. G. FATELEY, F. R. DOLLISH, N. T. McDEVITT, AND F. F. BENTLEY, Infrared and Raman Selection Rules for Molecular and Lattice Vibrations: The Correlation Method, Wiley–Interscience, New York (1972).

34. F. ABRAHAM, M. F. DEBREUILLE-GRESSE, G. MAIRESSE, AND G. NOWOGROCKI, *Solid State Ionics* **28–30,** 529 (1988).

35. D. J. BUTTREY, D. A. JEFFERSON, AND J. M. THOMAS, *Philos. Mag. (A).* **53** 897 (1986).

36. A. WATANABE, S. HORIUCHI, AND H. KODAMA, *J. Solid State Chem.* **67** 333 (1987).

37. D. C. CRAIG AND N. C. STEPHENSON, *J. Solid State Chem.* **15,** 1 (1975).

38. I. D. BROWN AND K. K. WU, *Acta Crystallogr.* **B32,** 1957 (1976).

39. G. DEO, F. D. HARDCASTLE, M. RICHARDS, AND I. E. WACHS, *ACS Petroleum Chemistry Division Preprints* **34(3),** 529 (1989).